Geophys. J. Int. (1999) **136,** 8–18

Mechanisms for the formation of ridge-axis topography at slow-spreading ridges: a lithospheric-plate flexural model

Y. John Chen[1] and Jian Lin[2]

[1] *College of Oceanic and Atmospheric Sciences, Oregon State University, Corvallis,* OR 97331, *USA*
[2] *Department of Geology and Geophysics, Woods Hole Oceanographic Institution, Woods Hole,* MA 02543, *USA*

Accepted 1998 June 4. Received 1998 April 12; in original form 1997 June 15

SUMMARY

The seafloor topography of a slow-spreading ridge shows a number of well-documented regularities at the ridge segment scale as the result of the complex interplay between ridge-axis magmatic and tectonic processes. This paper describes the results of a detailed analysis of the seafloor topography of the Mid-Atlantic Ridge near the Atlantis transform, where marine gravity data provide independent, although non-unique, constraints on subseafloor density structure. Using a combined topography and gravity data set, we identified the specific contributions of subseafloor density structure to the seafloor topography. We show that the observed along-axis deepening (0.3–0.8 km) from the midpoint of a ridge segment towards the non-transform offsets in the study area can be explained by the vertical deflection of a zero-age plate in response to along-axis crustal thickness variations. However, this effect can only account for 50–60 per cent of the observed 1.5–1.7 km deepening towards the Atlantis transform, suggesting the presence of significant stresses in the lithosphere near a transform. Results of plate flexural calculations also predict a more elevated rift flank at the inside corner of the ridge–transform intersection than at the conjugate outside corner. Such an asymmetry in rift flank topography is calculated to be greatest near a transform fault with a significant volume of deep transform valley and when adjacent plates across the transform fault are mechanically decoupled or only weakly coupled. Together these results illustrate the complex interplay between various tectonic processes at a slow-spreading ridge.

Key words: lithospheric plate flexure, slow-spreading ridges, transform faults.

1 INTRODUCTION

Over the past two decades, a substantial portion of the slow-spreading Mid-Atlantic Ridge (MAR) has been mapped by multibeam bathymetry and side-scan sonars, revealing significant variations in seafloor topography and faulting patterns along the ridge axis (e.g. Searle 1979; Macdonald 1982; Fox & Gallo 1984; Macdonald, Sempere & Fox 1984; Lonsdale 1989; Sempere, Purdy & Schouten 1990; Sempere *et al.* 1993; Fox, Grindlay & Macdonald 1991; Grindlay, Fox & Macdonald 1991; Carbotte & Macdonald 1992; Shaw & Lin 1993). The seafloor topography of a slow-spreading ridge shows a number of well-documented regularities at the ridge segment scale: (1) the seafloor is often most elevated at the midpoint of a segment but deepens systematically towards segment offsets; (2) the rift flank topography is most symmetric at the segment midpoint but becomes highly asymmetric near ridge offsets, where the inside-corner crust is found to be systematically elevated relative to that of the outside corner; (3) the spacing and throw of rift-bounding normal faults appear to be smallest at segment midpoints but increase towards segment offsets; and (4) large-amplitude normal faults tend to be located at inside corners. In addition to the topographic changes, gravity and seismic evidence suggests that the crustal structure also changes significantly within a ridge segment, with thicker crust at the segment centre and thinner crust at the distal ends (e.g. Lin & Phipps Morgan 1992; Tolstoy, Harding & Orcutt 1993; Detrick, Needham & Renard 1995).

A number of alternative mechanisms have been proposed to explain the above regularities in seafloor topography. For example, Sleep & Biehler (1977) and Parmentier & Forsyth (1985) postulated the viscous resistance of a transform wall to the upwelling mantle within a rift valley as the primary mechanism of seafloor deepening towards a transform fault. Several different mechanisms have also been proposed for the origin of inside-corner uplift, including non-linear viscoelastic rheology of the lithosphere (Bercovici, Dick & Wagner 1992), kinematic differences between the active and inactive portions

of a fracture zone (Kuo, Morgan & Forsyth 1984; Severinghaus & Macdonald 1988; Grindlay & Fox 1993; Escartin & Lin 1995), and unevenly distributed frictional stresses across the active transform fault (Chen 1989). While each of these mechanisms could qualitatively explain certain aspects of the observed regularities in seafloor topography, none of these models had considered the new gravity and seismic data that provide direct evidence for significant variations in subseafloor density structure within a ridge segment. These lateral variations in crustal and mantle density structure must exert significant influence on the seafloor topography, although their specific effects are poorly understood.

This paper describes the results of a detailed analysis of the seafloor topography of the Mid-Atlantic Ridge near the Atlantis transform, where marine gravity data provide independent, although non-unique, constraints on subseafloor density structure. Using the combined topography and gravity data set and a plate flexural model, we attempted to identify the specific components in the seafloor topography that are caused by subseafloor density anomalies and those that are generated by other processes. Results of this study suggest that subseafloor density anomalies contribute primarily to along-axis seafloor depth changes in most segments bounded by non-transform offsets, while dynamic processes associated with the formation of transform and rift valleys must be responsible for the additional seafloor deepening towards a transform. Together these results illustrate the complex interplay at the segment scale between various tectonic processes of a slow-spreading ridge. Table 1 lists the notations used throughout the text.

2 THE MID-ATLANTIC RIDGE

We choose the extensively studied area of the northern Mid-Atlantic Ridge between 27.9°N and 30.6°N (Fig. 1a) to test different loading models. The tectonic setting of the study area has been well documented from Sea Beam, magnetic and gravity surveys (Purdy *et al.* 1990; Sempere *et al.* 1990, 1993; Lin *et al.* 1990). It contains six 20–80 km long active spreading segments that are offset by the Atlantis transform (69 km) and four non-transforms (< 30 km) (Fig. 1a). While the off-axis morphology shows similar degrees of variation (e.g. Pariso, Sempere & Rommevaux 1995; Tucholke *et al.* 1997), we focus primarily on the near-ridge-axis region (< 3 Myr), where the oceanic lithosphere is thinnest and thus its deformation is most active.

Because there is no direct measurement of seismic crustal thickness in the study area, we used a gravity-derived model as a first-order approximation. Residual mantle Bouguer anomalies (RMBAs) were obtained by removing the predictable gravitational attraction due to the water–crust interface (density contrast of 1700 kg m^{-3}), the crust–mantle interface (density contrast of 600 kg m^{-3}) and mantle lithospheric cooling from the shipboard free-air gravity anomalies (Kuo & Forsyth 1988; Lin *et al.* 1990). Positive RMBAs indicate areas of relatively thin crust or cold mantle (mass excess), and more negative RMBAs indicate areas of relatively thick crust or hot mantle (mass deficit). Either crustal or mantle density variations should generate seafloor topography by creating buoyancy forces acting on the young oceanic lithosphere. Fig. 1(b) shows a map of gravity-derived crustal thickness, assuming that RMBAs are caused only by crustal thickness

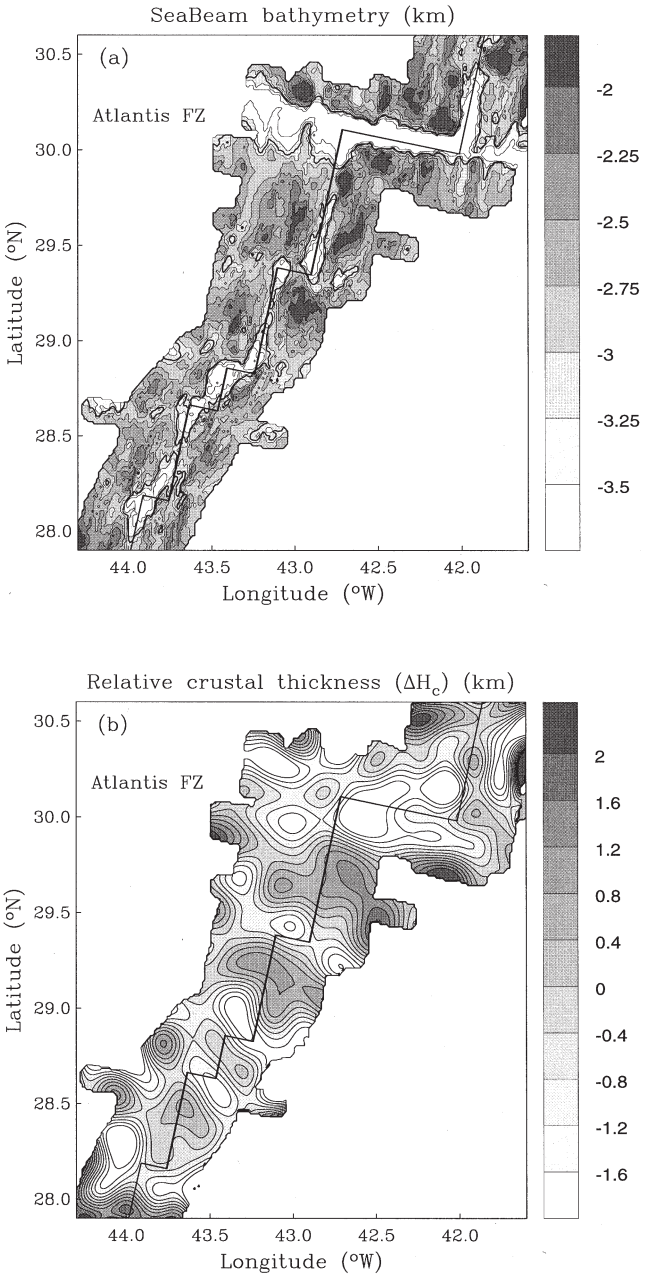

Figure 1. (a) Sea Beam bathymetry map of the north MAR between 27.5° and 30.7°N. The original Sea Beam bathymetric data have been interpolated onto a 1 km grid and machine-contoured at 250 m intervals. The ridge axis as determined by bathymetry and magnetic data contains six 20–80 km long active spreading segments that are offset by the Atlantis transform (69 km) and four non-transforms (< 30 km). Data from Sempere *et al.* (1990). (b) Contour map of crustal thickness variations of the study area. It is derived by downward continuation of the residual gravity anomalies (Fig. 2d of Lin *et al.* 1990) from sea level to the 6 km depth of Moho from the seafloor. Notice the thin crust at both inside corners flanking the Atlantis transform and also at the inside corners of non-transform features at 28°42′, 28°51′N and 29°23′N.

deviations from the 6 km global average (Chen 1992). Table 2 lists the observed along-axis seafloor relief and gravity-derived crustal thickness variations along the six segments. (The segment numbers correspond to those shown in Fig. 4.)

Table 1. Notation.

Variable	Meaning	Value	Units
ρ_w	Sea-water density	1030	kg m^{-3}
ρ_c	Crustal density	2700	kg m^{-3}
ρ_m	Mantle density	3300	kg m^{-3}
α	Thermal expansion coefficient	3.4×10^{-5}	°C^{-1}
E	Young's modulus	7×10^9	Pa
g	Acceleration of gravity	9.8	m s^{-2}
t_e	Effective elastic plate thickness	1 or 5	km
W_R	Width of model rift valley	15	km
D_R	Depth of model rift valley	1.0	km
W_T	Width of model transform valley	15	km
D_T	Depth of model transform valley	1.5	km
F	Buoyancy force		N
L	Segment length		km
$\Delta H_c = 2\Delta h_c$	Segment-scale variation in crustal thickness		km
$\bar{H}_c$	Average crustal thickness in a segment		km
ΔT	Mantle temperature variation		°C

Table 2. Along-axis variability in seafloor depth.

Segment[1] No.	Segment length (km)	Observed relief (km)	Predicted relief (1 km thick plate) (km)	Predicted relief (5 km thick plate) (km)	Crust[2] thickness variation (km)	Offset type
1S	75	1.5	0.8	0.7	1.6	Transform
2N	85	1.7	1.0	0.8	1.8	Transform
2S	85	1.0	1.0	0.8	1.8	Non-transform
3N	63	0.6	0.7	0.5	1.4	Non-transform
3S	63	0.9	0.7	0.5	1.4	Non-transform
4N	24	0.3	0.3	0.2	0.5	Non-transform
4S	24	0.3	0.2	0.0	0.5	Non-transform
5N	57	0.5	0.6	0.4	1.1	Non-transform
5S	57	0.7	0.6	0.4	1.1	Non-transform
6N	60	0.7	0.6	0.5	1.2	Non-transform

[1] N denotes northern half-segment; S denotes southern half-segment.
[2] Gravity-derived along-axis crustal thickness variation within a segment.

Since the interpretation of gravity data is non-unique, the gravity-derived crustal thickness provides only an end-member estimation, in which all RMBA signals are assumed to arise in the crust–mantle interface. The predicted buoyancy forces based on the RMBA-derived crustal thickness map would underestimate the actual buoyancy forces if the actual density anomalies lay deeper than the assumed Moho source depth. Likewise, this approach will overestimate buoyancy forces if the actual density anomalies lie shallower than the Moho. While there is a trade-off between the assumed source depth of gravity anomalies and the predicted amplitude of buoyancy forces, the predicted spatial patterns of positive and negative buoyancy loads are nevertheless independent of the assumed source depth.

It has been documented in the Atlantic that there is a linear correlation between the amplitude of spreading-segment RMBA variations and the segment length (Lin *et al.* 1990; Detrick *et al.* 1995). Thus it is also expected that there exists a similar linear correlation between the gravity-derived crustal thickness variations (ΔH_c) and the segment length (L). Fig. 2 shows the combined data from two study areas of MAR 33–37°N (Detrick *et al.* 1995) and MAR 28–31°N (Lin *et al.*

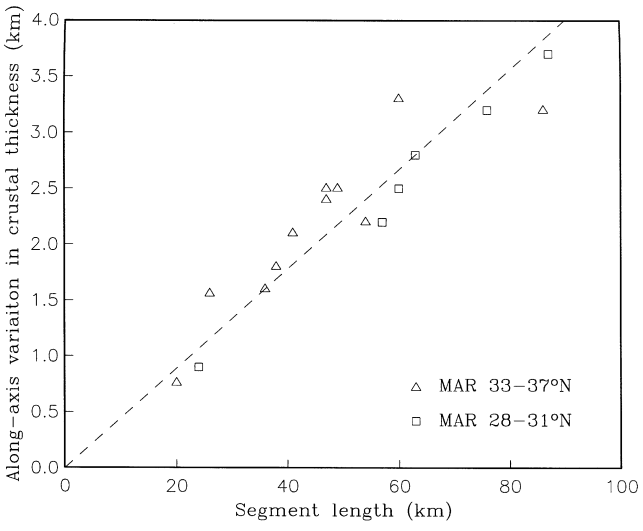

Figure 2. Relationship between the maximum crustal thickness variations along a ridge segment and the segment length. Data shown in triangles are from 33 to 37°N of the MAR (Detrick *et al.* 1995) and data shown in squares are from this study area (Lin *et al.* 1990). The dashed line is the best-fit linear regression of the combined data.

1990). Linear regression yields

$$\Delta H_c(L) = 0.0206L\,(\mathrm{km}). \quad (1)$$

Eq. (1) will be used in the subsequent model calculations for describing the ideal crustal thickness variation along a ridge segment of length L.

3 MODEL

Flexural response of the oceanic lithosphere has been previously proposed for creating ridge-axis morphology. For example, flexure of a thin oceanic lithosphere by low-density anomalies beneath a fast-spreading ridge has been shown to produce an axial topographic high at the East Pacific Rise (Madsen, Forsyth & Detrick 1984; Madsen *et al.* 1990; Wang & Cochran 1993; Wang, Cochran & Barth 1996; Magde, Detrick & the TERA Group 1995). However, Eberle & Forsyth (1998) recently have proposed an alternative model for the axial high in which the axial high topography is balanced by the dynamic moments within the crust resulting from the extensional stresses at the ridge axis. Here we consider a similar finite-element plate model to calculate the flexural deflection of the oceanic lithosphere in response to various types of vertical tectonic forces in a slow-spreading environment.

3.1 Vertical forces

We idealize the oceanic lithosphere as a thin elastic plate overlying a stress-free (mantle) fluid substratum (Fig. 3). Vertical forces due to temperature-related density variations in the mantle half-space, $\Delta T(x, y, z)$, and due to variations in crustal thickness, $\Delta H_c(x, y)$, are formulated as 'subseafloor loads' acting on the lithospheric plate:

$$F_{\mathrm{subseafloor}}(x, y) = -\alpha\rho_m g \int \Delta T(x, y, z)\, dz + (\rho_m - \rho_c) g \Delta H_c(x, y), \quad (2)$$

where ρ_m and ρ_c are the mantle and crustal density, respectively, g is gravity, α is the thermal expansion and ΔT is the temperature variation.

The deep rift and transform valleys commonly observed at slow-spreading ridges also exert vertical forces on top of the lithospheric plate and are referred to as 'seafloor loads':

$$F_{\mathrm{seafloor}}(x, y) = \begin{cases} (\rho_c - \rho_w) g D_R(x, y) & \text{within rift valley} \\ (\rho_c - \rho_w) g D_T(x, y) & \text{within transform valley} \\ 0 & \text{outside rift and transform valleys} \end{cases}, \quad (3)$$

where ρ_w is the sea-water density, and $D_R(x, y)$ and $D_T(x, y)$ denote the depth of rift and of the transform valleys (Fig. 3), respectively. The deflection of the lithospheric plate in response to the vertical forces of eqs (2) and (3) were calculated using a finite-element code (Chen 1989) based on Reissner–Mindlin plate theory (Hughes 1987).

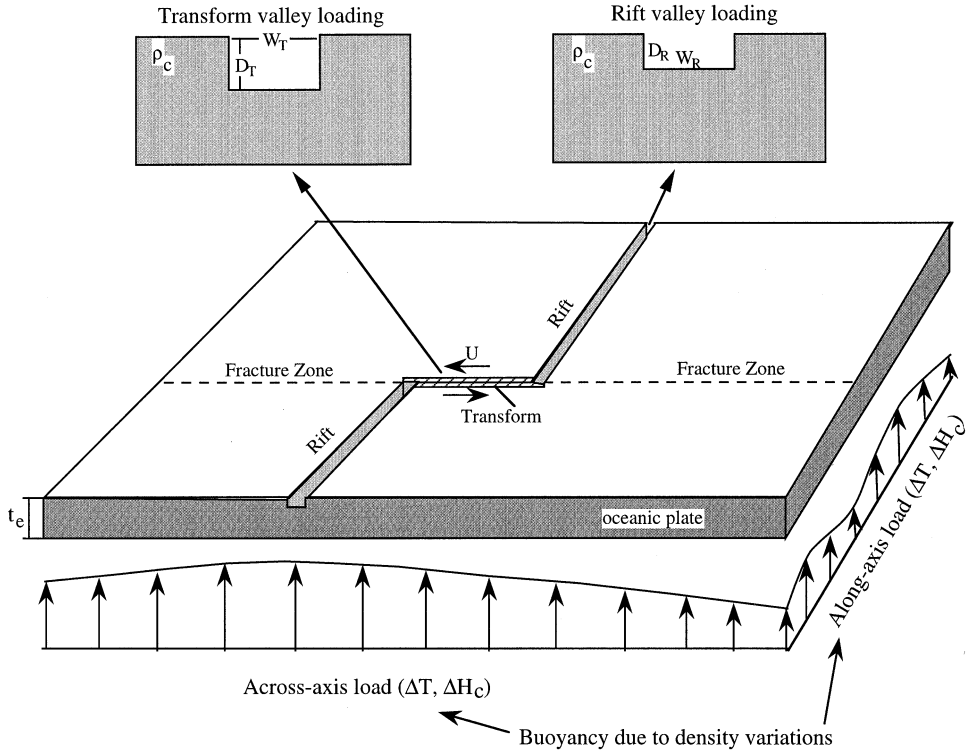

Figure 3. Schematic illustrating the different subseafloor and seafloor loads that may contribute to the topography of a slow-spreading ridge. The subseafloor loads include buoyancy forces due to lateral variations in mantle temperature and crustal thickness. The seafloor loads are the mass deficit from both the rift and the transform valleys. Note that the oceanic lithosphere is assumed to be an elastic plate with a constant effective elastic plate thickness (t_e).

3.2 Boundary conditions

Within the lithospheric plate, a staircase ridge–offset–ridge geometry was used to approximate the discrete MAR ridge segments (Fig. 4). Both the ridge axis and the transform fault were treated as zero-strength cracks incapable of transmitting shear stresses; friction along the transform fault was not considered here. The crack elements have a very large aspect ratio (several kilometres long and a few hundred metres wide) and almost zero elastic strength of $E = 7 \times 10^2$ Pa compared to $E = 7 \times 10^9$ Pa for the rest of the plate (where E is the Young's modulus). Far-field ridge-parallel boundaries are chosen to be sufficiently far away from the ridge axis to minimize their influence on the area of interest (Fig. 4). Experiments with alternative choices of fixed displacement and free stress conditions at these boundaries yielded similar results. The far-field transform-parallel boundaries are assumed symmetric about their axis. Finite element grids (ticks on edges of Fig. 4) were designed to be most dense at the ridge axis and near the ridge–offset intersections to ensure computational accuracy.

4 RESULTS

In this section, we have examined in detail the predicted deflection of the lithospheric plate in response to either separate or combined effects of mantle temperate, crustal thickness variations (eq. 2), and the presence of rift and transform valleys (eq. 3).

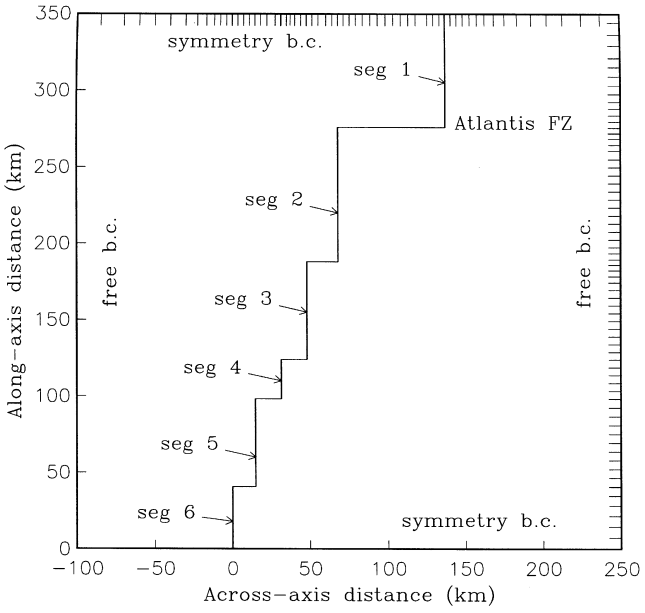

Figure 4. Geometry and boundary conditions of the finite-element flexural plate model. The finite-element grid mesh is shown as short ticks on the upper and right boundaries and calculations were carried out in a larger domain (x: 200–350 km; y: 50–400 km) than that shown here. Free-stress, or fixed-displacement, conditions are assumed for the off-axis boundaries. The upper and lower edges are treated as symmetric mirror boundaries to ensure continuity of the model ridge geometry. The ridge axis is modelled as shear-stress free crack elements (a broken-plate model), reflecting the relative weakness of the axial neovolcanic zone. Crack elements are also assigned for the Atlantis transform to simulate various mechanical coupling conditions. Non-transform offsets, however, are assigned continuous boundary conditions due to the absence of through-going strike-slip faults.

4.1 Effect of mantle temperature variations (ΔT)

The thermal subsidence history of the global ocean basins follows the relatively well-defined square-root-of-age relationship (Parsons & Sclater 1977; Stein & Stein 1992). Near a large-offset transform, however, the seafloor may subside more rapidly near the ridge axis because of additional heat loss across the transform (Chen 1988; Phipps Morgan & Forsyth 1988). A theoretical estimation of the mantle temperature field $\Delta T(x, y, z)$ in the study area was calculated numerically using a 3-D thermal model of passive mantle upwelling (Phipps Morgan & Forsyth 1988). Fig. 5(a) shows the predicted vertical deflection of a 1 km thick lithospheric plate in response to vertical forces associated with mantle-temperature (ΔT)-related density variations (the first term on the right-hand side of eq. 2).

The predicted seafloor deepening along the ridge axis from segment midpoints towards non-transform offsets is less than 50 m, and that towards the Atlantis transform is less than 100 m. The predicted topographic variation over the entire study area is less than 300 m, suggesting that mantle density variations associated with 3-D passive upwelling contribute only a small component to along-axis topographic variations in crustal age less than 20 Myr.

4.2 Effect of crustal thickness variations (ΔH_c)

On the basis of the observed linear relationship between crustal thickness and segment length (eq. 1), we adopted an idealized cosine shape of along-axis crustal thickness variation, $H_c(y)$, similar to that of Shaw & Lin (1996):

$$H_c(y) = \bar{H}_c + \Delta H_c \cos(\pi y/L)/2, \quad (4)$$

where L is the segment length, y is the along-axis distance from the segment midpoint and ΔH_c is the difference between the maximum and minimum values of crustal thickness along a segment (see Table 2 for ΔH_c values of the study area). The average crustal thickness $\bar{H}_c$ is chosen such that crustal thickness is continuous at segment boundaries.

The calculated vertical deflections of a 1 km thick lithospheric plate in response to the vertical forces of the idealized crustal thickness as described in eq. (4) are shown in Fig. 5(b). The deflection pattern is characterized by maximum uplift at the midpoint of each segment and minimum values at the segment ends. The predicted seafloor depth changes within a segment are in the range of 0.2–0.8 km, with the longer segment having greater depth relief. The predicted along-axis seafloor relief thereby is much greater because of the effect of crustal thickness variations (Fig. 5b) than because of mantle-temperature-related density variations (Fig. 5a).

4.3 Predicted zero-age depth variations

Combining the effects of mantle temperature variations (ΔT) and crustal thickness variations (ΔH_c) produces 'stripe'-shaped topographic corridors (Fig. 6a) of elevated seafloor along the off-axis continuation of segment midpoints bounded by the off-axis continuation of offsets. Along the axis of segments bounded by non-transform offsets, the predicted deflection of

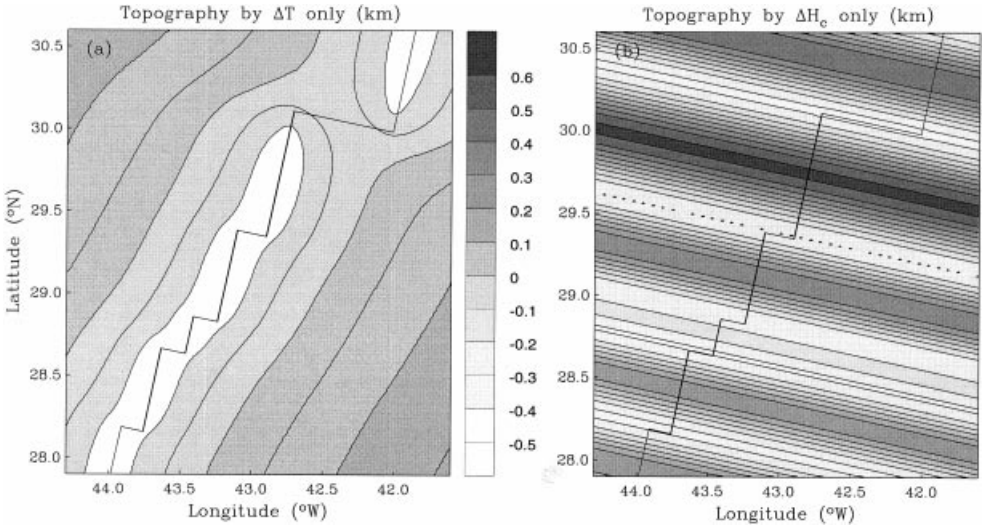

Figure 5. (a) Calculated flexural topography of an elastic plate (5 km thick) under thermal loads. The thermal buoyancy forces are from the temperature variations calculated using a 3-D passive-mantle-upwelling temperature model of Phipps Morgan & Forsyth (1988). (b) Calculated flexural responses of an elastic plate (5 km thick) under the buoyancy forces from the assumed model crustal thickness variations of eq. (4) along the six segments of our study area.

a 1 km thick lithospheric plate matches well the observed zero-age depth changes of 0.3–0.8 km (Table 2 and Fig. 7). The predicted deflection at the zero-age crust is somewhat smaller (by about 100 m) for a model with a 5 km thick lithospheric plate (Figs 6c and 7). These results suggest that the observed deepening of the seafloor from the segment midpoint towards non-transform offsets can be well explained by the deflection of the weak zero-age crust in response to crustal thickness and mantle temperature variations.

Towards the Atlantis transform, however, the predicted deflection of the zero-age crust due to the combined effects of the model ΔT and ΔH_c significantly underestimate the observed deepening of the seafloor by 600–800 m (Table 2 and Fig. 7). These results demonstrate the contrasting tectonics between non-transform and transform offsets: additional dynamic forces, such as that of mantle viscous head losses (Sleep & Biehler 1970; Parmentier & Forsyth 1985), might be required to explain the increased seafloor deepening towards major transform faults but are not required for smaller non-transform offsets.

For comparison, the plate deflections in response to the combined loads of temperature variations (Fig. 5a) and the actual gravity-derived crustal thickness variations (Fig. 1b) are shown in Figs 6(b) and (d) for 1 km and 5 km thick plates, respectively.

4.4 Residual topography

We derived a map of residual topography (Fig. 8a) by subtracting the predicted effects (Fig. 6b) of gravity-derived crustal thickness and mantle temperature variations from the observed seafloor topography (Fig. 1a). Comparison of Fig. 8(a) with Fig. 1 reveals two interesting features. First, the segment-centre upward bulges noted in the Sea Beam data are no longer present in the residual topography except for some residual features approaching the Atlantis transform fault. This indicates that the deepening of the rift valley floor towards non-transform offsets can indeed be attributed primarily to the flexural response of the zero-age plate due to buoyancy effects of crustal thickness and mantle temperature variations.

The second interesting feature is that the residual topography is mostly symmetric across the midpoint of spreading segments but becomes strongly asymmetric near ridge–offset intersections (Fig. 9). The elevated crust at both inside corners near the Atlantis transform is composed of a series of individual highs (marked as in Fig. 8a). Asymmetry is also observed near the non-transform offsets (Figs 8a and 9) but to a lesser degree. Other studies also noted that the degree of rift asymmetry is greater near transforms than near non-transform offsets along other sections of the Mid-Atlantic Ridge (e.g. Severinghaus & Macdonald 1988; Escartin & Lin 1995).

4.5 Asymmetric flexural response near a ridge–offset intersection

We next consider the deflection of the lithospheric plate in response to negative seafloor loads associated with rift and transform valleys. Although a number of alternative dynamic mechanisms may be responsible for the creation of a deep rift valley, including mantle viscous head loss (e.g. Sleep 1969; Lachenbruch 1976) and lithospheric stretching (e.g. Tapponnier & Francheteau 1978; Phipps Morgan, Parmentier & Lin 1987; Chen & Morgan 1990; Neumann & Forsyth 1993), the flexural response of the lithospheric plate is sensitive only to the volume of the rift valley and not the specific rifting mechanism. In our example calculations, the model rift valley was assumed to have a width of $W_R = 15$ km and a depth of $D_R = 1$ km.

A transform valley was similarly assumed to be generated dynamically (e.g. Pockalny, Gente & Buck 1995) and a simple geometry of $W_T = 15$ km and $D_T = 1.5$ km was used in example calculations. The predicted deflection of the lithospheric plate in response to these negative loads is shown in Fig. 10(a) for a 5 km thick plate. The most notable feature in the predicted topography is the presence of transverse ridges at the inside-corner crust on both flanks of the transform valley and the

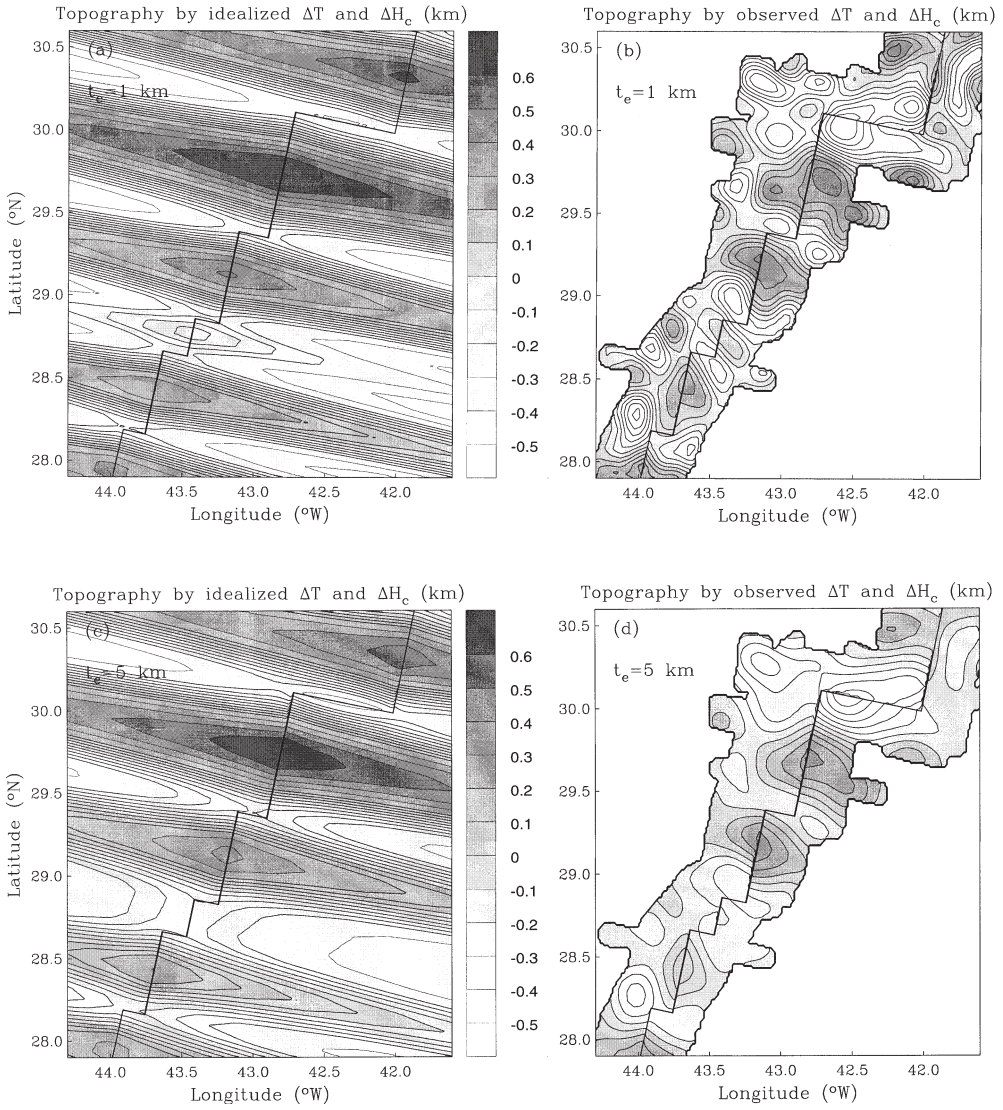

Figure 6. Calculated flexural responses of an elastic plate to subseafloor loads. Shown in (a) ($t_e = 1$ km) and (c) ($t_e = 5$ km) are plate deflections under the buoyancy forces from both the assumed model crustal thickness variations (eq. 4) and the mantle temperature variations. Shown in (b) ($t_e = 1$ km) and (d) ($t_e = 5$ km) are plate deflections under the buoyancy forces from both the gravity-derived crustal thickness variations (Fig. 1b) and the mantle temperature variations. Only the calculated deflections within the survey area of Fig. 1(b) are shown in (b) and (d).

absence of such ridges at the outside-corner crust (Figs 10a and 11). The amplitude of asymmetry in the rift flank topography is predicted to increase with increasing volume of the transform valley and decreasing degree of mechanical coupling across the transform fault.

The observed difference in faulting style (spacing, throw, etc.) between the segment midpoint and distal ends has been used to suggest that long periods of amagmatic extension are dominant, mostly near segment ends (e.g. Shaw & Lin 1993). We propose that during each amagmatic rifting episode, a low-angle detachment fault system is developed preferably at the inside corner of a ridge–transform intersection because of the presence of a relatively weak transform fault compared to that at the outside corner. The faulting-created topography at the inside corner is then carried away along the fracture zone walls and is supported by a growing lithospheric plate. Indeed, these inside-corner highs shown in the residual topography (Fig. 8a) can be traced a long distance in the off-axis Sea Beam topography (Tucholke *et al.* 1997).

Fig. 10(b) shows the predicted deflection of a 5 km thick plate in response to the combined effects of crustal thickness variations, mantle temperature changes and the presence of rift and transform valleys. In general, this model topography reflects well the long-wavelength features in the observed seafloor bathymetry along and near the ridge axis (Fig. 1). In particular, the doming of the rift valley seafloor at the centres of the longer segments is well captured in the combined model topography.

4.6 Coupling conditions at transform faults

To explore further the dependence of the rift asymmetry on either the offset length or the mechanical conditions of a transform fault, we conducted a suite of numerical experiments

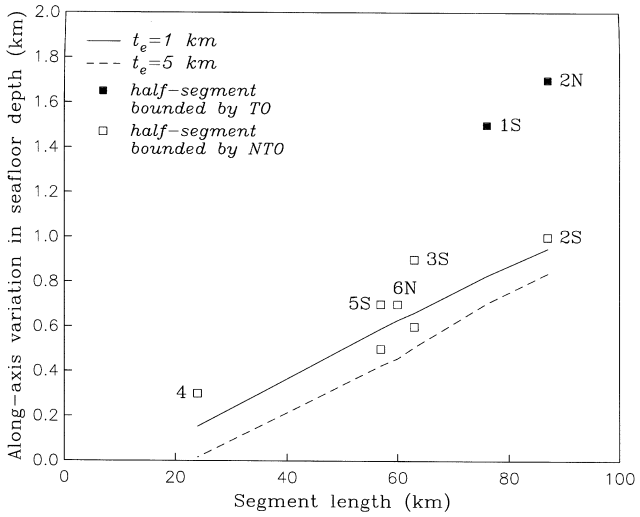

Figure 7. Relationship between the seafloor depth variations along a ridge segment and the segment length. Data shown in squares are from Lin *et al.* (1990). The variations are measured from the segment centre to one of the segment ends and, thus, there are two measurements for each segment. These data, in general, follow a linear trend except for the two measurements towards the Atlantis transform (1S and 2N) that have anomalously large amplitudes. The model calculations (measured along each segment from Fig. 6) are also shown as a solid line for $t_e = 1$ km and a dashed line for $t_e = 5$ km.

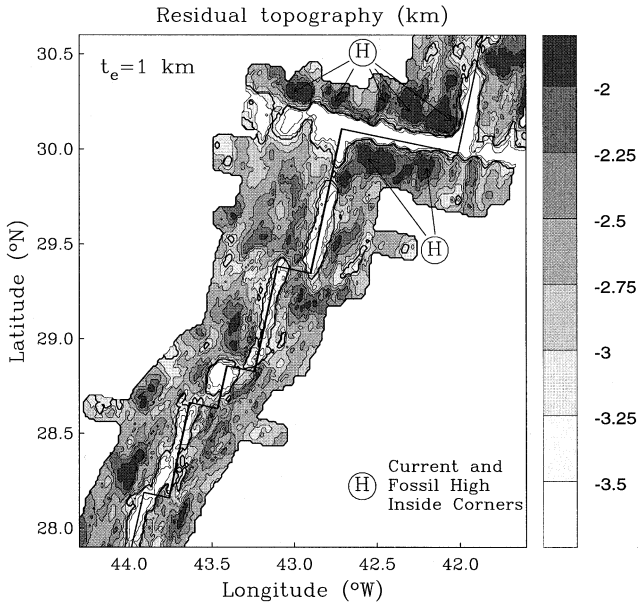

Figure 8. Residual topography derived by subtracting the subseafloor buoyancy effects (Fig. 6b) from the observed Sea Beam bathymetry (Fig. 1a) for $t_e = 1$ km. Note that both the axial rift valley and the Atlantis transform valley remain as well-connected systematic topographic lows, indicating their stress-supported dynamic origin. The most prominent topographic highs are observed over the current, as well as fossil, inside corners near the ridge–Atlantis transform intersections. Small inside-corner highs are also observed over the inside corners near non-transform offsets (see also Fig. 9a). We propose that during each amagmatic rifting episode, a high inside corner is formed in response to the combined negative loads of the rift and transform valleys and is enhanced by the weakness of the transform fault.

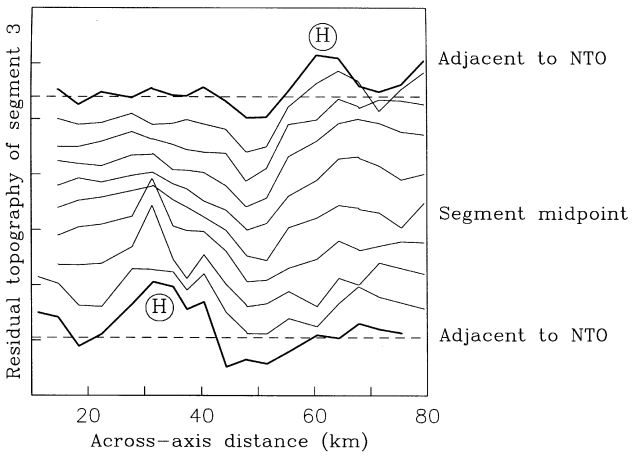

Figure 9. Across-axis profiles of residual topography shown in Fig. 8(a) along the segment 3 which is bounded by two non-transform offsets (see Fig. 4). The profile varies from symmetric at the segment midpoint to asymmetric approaching both segment ends, where an inside-corner uplift (H) is clearly identified.

with different offset lengths and coupling conditions across the transform (Fig. 12). The dotted line shows model calculations with a broken transform fault, i.e. the two plates are completely decoupled along the transform fault but are welded along the inactive fracture zone. The dashed line shows model calculations with a completely coupled transform, i.e. the plates are welded together along both the transform and the inactive fracture zone.

Both sets of calculations predict that the asymmetry in flexural deflection across the ridge axis is independent of the offset length (L) for $L > 50$ km. This is because the asymmetry is largely defined by the inside-corner uplift (Fig. 11), which depends mainly on the loads of the transform valley near a ridge–transform intersection. For a transform with an offset length that is at least 2–3 times the width of the rift valley W_R, there is little interaction between the crust at the two ends of the active transform fault. For shorter transforms, however, the inside-corner uplift on one end of the transform could feel the effect of the other transform end. Since most of the major transforms with a transform valley have an offset length greater than 50 km, we conclude that the asymmetry due to the loading of the transform valley is independent of the transform offset length. Similarly, the rift flank asymmetry is predicted to be independent of spreading-segment length when its value is greater than 2–3 times of the width of the rift valley. The predicted asymmetry for the case of a completely broken transform (dotted line) is about twice that for the case of an unbroken transform (dashed). Thus the mechanical conditions of the transform fault are an equally important factor in controlling the amplitude of the inside-corner uplift and the resultant asymmetry in rift flank topography.

Also shown in Fig. 12 are the observations of the average rift asymmetry near several transform faults (filled squares) and non-transform offsets (open squares) in the Atlantic (Severinghaus & Macdonald 1988; Escartin & Lin 1995). It is interesting to note that while the non-transform offsets are shorter than the transforms, their associated asymmetries are comparable to those of the transforms. With the exception of

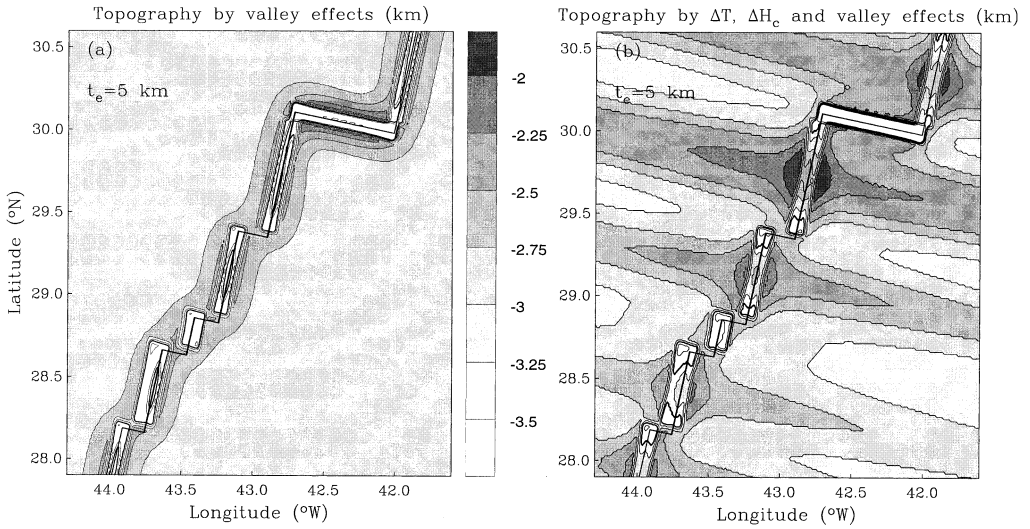

Figure 10. (a) Calculated flexural topography of an elastic plate ($t_e = 5$ km) in response to negative loads of rift and transform valleys. The geometry of such an initial surface load is shown in Fig. 3. Note that the predicted flexural uplift is quite symmetric at segment midpoints (also shown in Fig. 11). Approaching ridge-axis offsets, however, the rift flanks become asymmetric. The maximum asymmetric flanking uplift (0.8 km asymmetry) is predicted near the Atlantis transform. (b) Model topography of an elastic plate ($t_e = 5$ km) in response to combined seafloor and subseafloor loads (Fig. 3).

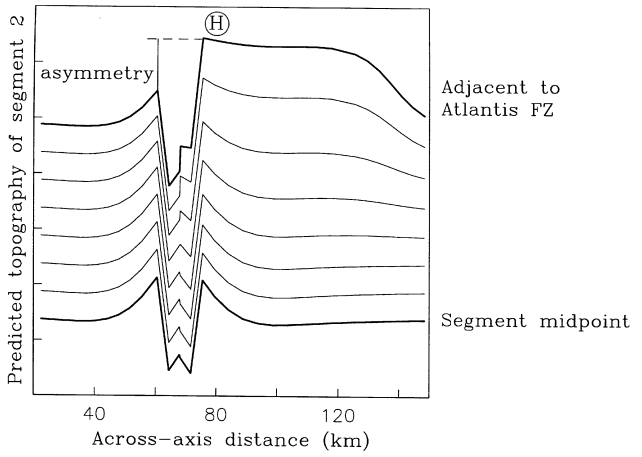

Figure 11. Across-axis profiles of plate deflections of Fig. 10(a) from the centre to the north end of the segment 2 where it offsets the Atlantis transform. Asymmetry is defined as the maximum topographic difference between the inside-corner and outside-corner rift flanks. Uplifts are developed at the inside-corner high (H) and along the Atlantis transform valley (see also Fig. 10a).

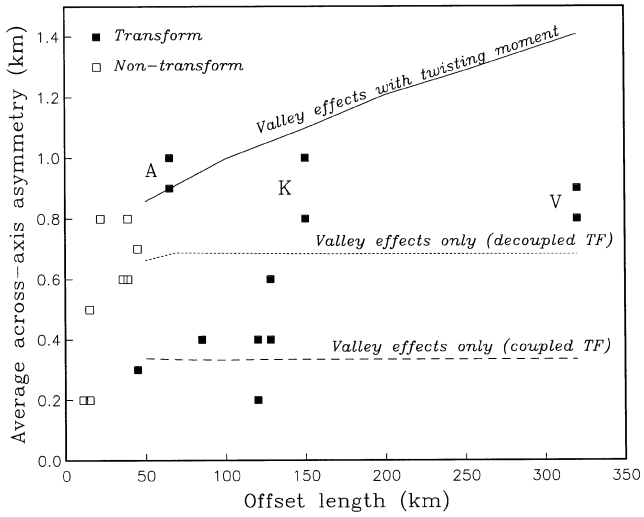

Figure 12. Plot of across-axis asymmetry versus the offset length. The data are shown for the transforms (filled squares) and non-transforms (open squares) in the Atlantic and are derived from calculations of Escartin & Lin (1995), except for the Vema transform from Severinghaus & Macdonald (1988). V – Vema transform; K – Kane transform; A – Atlantis transform. The calculated model asymmetry in response to negative loads of rift and transform valleys is shown for the case of a completely broken transform fault (dotted line) and a perfectly coupled transform (dashed line). Note that the asymmetry from these seafloor loads is predicted to be independent of the transform offset length with offset length greater than 50 km. The solid lines show the predicted asymmetry considering both a postulated twisting moment along the transform (Chen 1989) and negative loads of rift and transform valleys.

the large asymmetry associated with the Atlantis transform, there seems to be little correlation between offset length and magnitude of rift flank asymmetry.

In a previous study, Chen (1989) has investigated the dependence of inside-corner uplift on the magnitude of a twisting moment exerted along the transform fault. The twisting moment is caused by a linear increase in shear stress with depth (Byerlee's law) along the transform. The study has also considered the difference in plate coupling between the transform (weak) and the inactive fracture zone (strong). The solid line in Fig. 12 shows the combined effects (Chen 1989 and this study) assuming a completely broken transform fault. While the transform valley loading effect is predicted to contribute the most (>70 per cent) to the asymmetry at transforms such as the Atlantis and the Kane, the contribution from the twisting-moment mechanism increases with offset length.

5 DISCUSSION

The well-documented along-axis deepening of the rift valley floor towards segment ends has been previously attributed to dynamic origin, i.e. it reflects the along-axis variations in the rifting process which creates the rift valleys (e.g. Sleep 1969; Lachenbruch 1976; Parmentier & Forsyth 1985; Neumann & Forsyth 1993). As an alternative mechanism, we have shown in this study that most of the observed along-axis deepening of the seafloor towards the non-transform offsets can be explained adequately by the buoyancy effects of crustal thickness and mantle temperature variations (Fig. 7).

However, contributions from dynamic processes are required to account for the larger seafloor deepening towards the Atlantis transform (Fig. 7). We believe that there are at least three reasons for the importance of dynamic seafloor deepening towards a transform offset. First, because transforms usually have larger offsets than non-transform offsets, they cause larger perturbations to the ridge-axis thermal and rheological structures of the lithosphere. Second, dynamic rifting could be enhanced by the weak mechanical conditions of a transform fault. And finally, the dynamic process for the formation of the transform valley (e.g. Pockalny *et al.* 1995) may also contribute to the seafloor deepening towards a transform fault although such an effect is still poorly quantified.

6 CONCLUSIONS

The results of this study illustrate the complex interplay between various tectonic processes of a slow-spreading ridge. They lead to the following conclusions.

(1) The observed seafloor deepening towards a non-transform offset can be adequately explained by plate flexure in response to buoyancy forces arising from spatial variations in crustal thickness (first-order effect) and mantle temperature (second-order effect). The amplitude of the along-axis depth changes is predicted to increase with segment length as the result of the observed increase in the crustal thickness variability with segment length. While there is a trade-off between the assumed source depth of gravity anomalies and the amplitude of buoyancy forces, the predicted spatial patterns of positive and negative buoyancy loads are subjected to lesser uncertainties.

(2) Towards a well-developed transform fault such as the Atlantis, however, the observed seafloor deepening is substantially greater than that calculated on the basis of the crustal and mantle buoyancy effects alone. The differences in the observed and the calculated topography are attributed to other mechanisms responsible for the formation of rift and transform valleys.

(3) Rift flank topography is predicted to be most symmetric across the midpoint of a ridge segment but becomes highly asymmetric approaching a ridge–transform intersection with the inside-corner crust more elevated than the conjugate outside corner. Such an asymmetry in rift flank topography is calculated to be greatest near a transform fault with a significant volume of transform valley and when adjacent plates across the transform fault are mechanically decoupled or only weakly coupled. Within this study area, this mechanism explains qualitatively the observation that inside-corner uplift is in general greater near a transform fault such as the Atlantis, where the transform valley is deep and earthquakes indicate weak fault conditions, than near a non-transform offset, where a weak strike-slip fault with a valley is often absent. However, this correlation between the offset length and the asymmetry does not seem to hold when offsets from different parts of the Atlantic are compared with each other, suggesting that other tectonic variables, in addition to offset length, must also play a role in controlling the asymmetry between the inside- and outside-corner crust.

ACKNOWLEDGMENTS

We benefited from discussion with B. Tucholke, D. Smith and C. Ruppel. Marcia Turnbull helped with editing of the text. Two anonymous reviewers provided constructive comments on an earlier manuscript. This work was supported by NSF grant OCE-9300512 to YJC and NSF grant OCE-9300708 to JL. YJC was also supported by the College of Oceanic and Atmospheric Sciences at Oregon State University. WHOI contribution number 8619.

REFERENCES

Bercovici, D., Dick, H.J.B. & Wagner, T.P., 1992. Nonlinear visco-elasticity and the formation of transverse ridges, *J. geophys. Res.,* **97,** 14 195–14 206.

Carbotte, S.M. & Macdonald, K.C., 1992. East Pacific Rise 8°10′30′N: evolution of ridge segments and discontinuities from SeaMARC II and three-dimensional magnetic studies, *J. geophys. Res.,* **97,** 6959–6982.

Chen, Y., 1988. Thermal model of oceanic transform faults, *J. geophys. Res.,* **93,** 8839–8851.

Chen, Y., 1989. A mechanical model for the inside corner uplift at a ridge–transform intersection, *J. geophys. Res.,* **94,** 9275–9282.

Chen, Y., 1992. Oceanic crustal thickness versus spreading rate, *Geophys. Res. Lett.,* **19,** 753–756.

Chen, Y. & Morgan, W.J., 1990. A nonlinear-rheology model for mid-ocean ridge axis topography, *J. geophys. Res.,* **95,** 17 583–17 604.

Detrick, R.S., Needham, H.D. & Renard, V., 1995. Gravity anomalies and crustal thickness variations along the Mid-Atlantic Ridge between 33°N and 40°N, *J. geophys. Res.,* **100,** 3767–3787.

Eberle, M.A. & Forsyth, D.W., 1998. An alternative, dynamic model of the axial topographic high at fast-spreading ridges, *J. geophys. Res.,* **103,** 12 309–12 320.

Escartin, J. & Lin, J., 1995. Ridge offsets, normal faulting, and gravity anomalies of slow spreading ridges, *J. geophys. Res.,* **100,** 6163–6177.

Fox, P.J. & Gallo, D.G., 1984. A tectonic model for ridge–transform–ridge plate boundaries: implications for the structure of oceanic lithosphere, *Tectonophysics,* **104,** 205–242.

Fox, P.J., Grindlay, N.R. & Macdonald, K.C., 1991. The Mid-Atlantic Ridge (31°S–34°30′S): temporal and spatial variations of accretionary processes, *Mar. geophys. Res.,* **13,** 120.

Grindlay, N.R. & Fox, P.J., 1993. Lithospheric stresses associated with nontransform offsets of the Mid-Atlantic Ridge: implications from a finite element analysis, *Tectonics,* **12,** 982–1003.

Grindlay, N.R., Fox, P.J. & Macdonald, K.C., 1991. Second-order ridge axis discontinuities in the south Atlantic: morphology, structure, and evolution, *Mar. geophys. Res.,* **13,** 2149.

Hughes, T.J.R., 1987. *The Finite Element Method: Linear Static and Dynamic Finite Element Analysis,* Prentice-Hall, Englewood Cliffs, NJ.

Kuo, B.-Y. & Forsyth, D.W., 1988. Gravity anomalies of the ridge–transform system in the South Atlantic between 31° and 34.5°S: upwelling centers and variations in crustal thickness, *Mar. geophys. Res.,* **10,** 205–232, 1988.

Kuo, B.-Y., Morgan, W.J. & Forsyth, D.W., 1984. Asymmetry in topography of the crestal mountains near a ridge–transform intersection, *EOS, Trans. Am. geophys. Un.,* **65,** 274.

Lachenbruch, A.H., 1976. Dynamics of a passive spreading center, *J. geophys. Res.,* **81,** 1883–1902.

Lin, J. & Phipps Morgan, J., 1992. The spreading rate dependence of three-dimensional mid-ocean ridge gravity structure, *Geophys. Res. Lett.,* **19,** 13–16.

Lin, J., Purdy, G.M., Schouton, H., Sempere, J.-C. & Zervas, C., 1990. Evidence from gravity data for focused magmatic accretion along the Mid-Atlantic Ridge, *Nature,* **344,** 627–632.

Lonsdale, P., 1989. Segmentation of the Pacific-Nazca spreading center 1°N–20°S, *J. geophys. Res.,* **94,** 12 197–12 225.

Macdonald, K.C., 1982. Mid-ocean ridges: fine scale tectonic, volcanic, and hydrothermal processes within the plate boundary zone, *Ann. Rev. Earth planet. Sci.,* **10,** 155–190.

Macdonald, K.C., Sempere, J.C. & Fox, P.J., 1984. East Pacific Rise from Siqueiros to Orozco fracture zones: along-strike continuity of axial neovolcanic zone and structure and evolution of overlapping spreading centers, *J. geophys. Res.,* **89,** 6049–6069.

Madsen, J.A., Forsyth, D.W. & Detrick, R.S., 1984. A new isostatic model for the East Pacific crest, *J. geophys. Res.,* **89,** 9997–10 015.

Madsen, J.A., Detrick, R.S., Mutter, J.C., Buhl, P. & Orcutt, J.C., 1990. A two- and three-dimensional analysis of gravity anomalies associated with the East Pacific Rise at 9°N and 13°N, *J. geophys. Res.,* **95,** 4967–4987.

Magde, L.S., Detrick, R.S. & the TERA Group, 1995. Crustal and upper mantle contribution to the axial gravity anomaly at the southern East Pacific Rise, *J. geophys. Res.,* **100,** 3747–3766.

Neumann, G.A. & Forsyth, D.W., 1993. The paradox of the axial profile: isostatic compensation along the axis of the Mid-Atlantic Ridge?, *J. geophys. Res.,* **98,** 17 891–17 910.

Pariso, J.E., Sempere, J.-C. & Rommevaux, C., 1995. Temporal and spatial variations in crustal accretion along the Mid-Atlantic Ridge (29°31°30′N) over the last 10 m.y.: implications from a three-dimensional gravity study, *J. geophys. Res.,* **100,** 17 781–17 794.

Parmentier, E.M. & Forsyth, D.W., 1985. Three-dimensional flow beneath a slow spreading ridge axis: a dynamic contribution to the deepening of the median valley toward fracture zones, *J. geophys. Res.,* **90,** 678–684.

Parsons, B. & Sclater, J.G., 1977. An analysis of the variation of ocean floor bathymetry with age, *J. geophys. Res.,* **82,** 803–827.

Phipps Morgan, J. & Forsyth, D.W., 1988. Three-dimensional flow and temperature perturbations due to a transform offset: effects on oceanic crustal and upper mantle structure, *J. geophys. Res.,* **93,** 2955–2966.

Phipps Morgan, J., Parmentier, E.M. & Lin, J., 1987. Mechanisms for the origin of mid-ocean ridge axial topography: implications for the thermal and mechanical structure of accretion plate boundaries, *J. geophys. Res.,* **92,** 12 823–12 836.

Pockalny, R.A., Gente, P. & Buck, W.R., 1995. Oceanic transverse ridges: a flexural response to fracture-zone-normal extension, *Geology,* **24,** 71–74.

Purdy, G.M., Sempere, J.-C., Schouten, H., Dubois, D.L. & Goldsmith, R., 1990. Bathymetry of the mid-Atlantic ridge, 24°31°N: a map series, *Mar. geophys. Res.,* **12,** 247–252.

Searle, R.C., 1979. Side-scan sonar studies of North Atlantic fracture zones, *J. Geol.,* **136,** 283–292.

Sempere, J.-C., Purdy, G.M. & Schouten, H., 1990. Segmentation of the Mid-Atlantic Ridge between 24°N and 30°40′N, *Nature,* **344,** 427–429.

Sempere, J.-C., Lin, J., Brown, H.S., Schouten, H. & Purdy, G.M., 1993. Segmentation and morphotectonic variations along a slow-spreading center: the Mid-Atlantic Ridge 24°30°40′N, *Mar. geophys. Res.,* **9,** 153–200.

Severinghaus, J.P. & Macdonald, K.C., 1988. High inside corners at ridge–transform intersections, *Mar. geophys. Res.,* **9,** 353–367.

Shaw, P.R. & Lin, J., 1993. Causes and consequences of variations in faulting style at the Mid-Atlantic Ridge, *J. geophys. Res.,* **98,** 21 839–21 851.

Shaw, W. & Lin, J., 1996. Models of ocean ridge lithospheric deformation: dependence on crustal thickness, spreading rate, and segmentation, *J. geophys. Res.,* **101,** 17 977–17 993.

Sleep, N.H., 1969. Sensitivity of heat flow and gravity to the mechanism of sea-floor spreading, *J. geophys. Res.,* **74,** 542–549.

Sleep, N.H. & Biehler, S., 1970. Topography and tectonics at the intersections of fracture zones with central rifts, *J. geophys. Res.,* **75,** 2748–2752.

Stein, C.A. & Stein, S., 1992. A model for the global variation in oceanic depth and heat flow with lithospheric age, *Nature,* **359,** 123–129.

Tapponnier, P. & Francheteau, J., 1978. Necking of the lithosphere and the mechanics of slowly-accreting plate boundaries, *J. geophys. Res.,* **83,** 3955–3970.

Tolstoy, M., Harding, A.J. & Orcutt, J.A., 1993. Crustal thickness on the Mid-Atlantic Ridge: bull's eye gravity anomalies and focused accretion, *Science,* **262,** 726–729.

Tucholke, B.E., Lin, J., Kleinrock, M.C., Tivey, M.A., Reed, T.B., Goff, J. & Jaroslow, G.E., 1997. Segmentation and crustal structure of the western Mid-Atlantic Ridge flank, 25°25′27°10′N and 029 m.y., *J. geophys. Res.,* **102,** 10 203–10 223.

Wang, X. & Cochran, J.R., 1993. Gravity anomalies, isostasy, and mantle flow at the East Pacific Rise crest, *J. geophys. Res.,* **98,** 19 505–19 531.

Wang, X., Cochran, J.R. & Barth, G.A., 1996. Gravity anomalies, crustal thickness, and the pattern of mantle flow at the fast spreading East Pacific Rise, 9°10°N: evidence for three-dimensional upwelling, *J. geophys. Res.,* **101,** 17 927–17 940.